# CFD Analysis of Particle Shape and Size on Impact Velocity and Effect of Stand-off Distance in the Cold Spray Process


**Mohsin Khan, Mohammad Zunaid, and Qasim Murtaza**

**Abstract** The computational fluid dynamics (CFD) analysis is the latest technology, and also the accuracy is very close to the experimental analysis. In the present work, the effect of shape and size of feedstock powder particles is analyzed upon impact velocity of cold spray (CS) coating via CFD analysis. The geometry for the work has been drawn by SolidWorks, and the analysis has been carried out through fluent. The analysis has been carried out with the best input parameters for CS coating. The pressure-based; axisymmetric model has been used to solve the CS nozzle. The most realistic two-equation realizable k-ε model has been taken for the analysis. In this analysis, there is a range of particle diameter or varying particle sizes, and with varying the standoff distance from the nozzle, exit/outlet has been taken. The analysis is carried out using copper as the spray powder particles and steel as the substrate material. It has been found that the spherical shape of powder particles is more reliable when sprayed with a standoff distance of 35 mm.

**Keywords** CFD simulation · Cold spray · Impact velocity · Standoff distance · Particle shape

## 1 Introduction

In the cold spray (CS) coating process, the feedstock powder is sprayed with the help of a nozzle to get a high impact velocity or jet towards the substrate upon which coating is to be performed. With this coating process technology number of metals, composite materials, polymers, and ceramics can be coated based upon the applications and requirements. Nowadays, this coating technology is growing in the manufacturing industry by creating a dedicated branch in additive manufacturing called cold spray additive manufacturing, solid-state powder-based deposition process [1–3], and cold gas dynamic manufacturing [4].

M. Khan (✉) · M. Zunaid · Q. Murtaza
Department of Mechanical Engineering, Delhi Technological University, Bawana Road, Delhi 110042, India
e-mail: mohsindtu@gmail.com



A. Maurya et al. (eds.), *Recent Trends in Mechanical Engineering*, Lecture Notes in Mechanical Engineering, https://doi.org/10.1007/978-981-19-7709-1_11

Decrease of particle size to the nano-level, domination of surface roughness observed parallelly [5], residual stresses increases upon grinding in nanostructured coatings [6]. Powder material heat treatment increases the efficiency of deposition about two times and decreases the porosity about four times [7]. Cladded powders can be developed by covering the alumina particles with a nickel layer using the hydrogen reduction method [8]. Using CS technology compact nanocrystalline grains produced due to impact, moiré pattern was observed due to preserved tamping effect produced by microstructure, and there was no size change found in nano-sized grains [9]. The feasible and simple way for determining particle distribution of cold sprayed coated composites found to be the Weibull distribution method [10].

Using crystal orientation of particles on the coating surface with the help of molecular dynamics simulation, the shape of particles at the bottom edge is found of square-shape, rectangle-shape, and hexagon-shape [11]. The aerosol deposition (AD) method is also a type of CS coating process technique, in which ceramic coating formation and bonding were analyzed practically as well as using CFD simulations [12]. The molecular dynamic simulation gives the results with asymmetric particle deformation at the interface that occurred during cold gas spray [13]. The particle size of 40 μm founds gives high impact velocity as compared to the 20, 60, 80, and 100 μm particle sizes [14].

CS coated surface has compressive residual stresses because of deformation and particle impact at high velocity [15]. The newly developed model based on Johnson-Cook (JC) model can effectively predict the stresses and deformed shape of particles [16]. In CS process technology, the temperature of the powder particles also depends upon the injector length, the higher the injector length, the lower will be the temperature of particles and vice-versa [17]. The CS coating process gives high thermal conductivity and sensible adhesion strength [18]. The surface roughness of sintered alumina in comparison with alumina found to be lower [19] which affects the porosity, hardness, and density in outer and middle regions due to grain size reduction. The wear rate increases with an increase in the load [20]. Laser remelting decreases the porosity of thermal ceramic coatings, a significant effect as compare to as-sprayed coating exhibits upon various mechanical properties like microhardness, elastic modulus, etc. [21]. Crater formation found negligible upon hard metal substrates [22]. CS coating using composite powder gives low porosity and high hardness and fracture-toughness [23].

CS coatings with low temperature (500 °C) give the best corrosion resistance. Post deposition heat treatment improves bonding and porosity [24]. In comparison with uncoated material with aluminium and chromium coated, aluminium coated found to be better oxidation resistance at high working temperature environment [25]. Pulse plasma nitriding is not sufficient to improve corrosion resistance [26]. The pre-heat temperature in CS coating technology improves the first layer deposition which improves the bonding strength [27].

Critical velocity and coating quality improve with improving the impact velocity well above the critical velocity. In the presence of oxide, the particles jetting and flattening decrease [28]. Velocity or impact velocity affects the CS coating to an extent

[27]. Iron-based amorphous/nanocrystalline composite coatings exhibit better corrosion resistance as compared to galvanized steel with improved corrosion resistance and microhardness than steel substrate [28, 29]. Copper and copper-titanium dioxide coating using low-pressure CS coating technique give metallic and amorphous structure, respectively [30].

This research aims to improve the impact velocity and temperature of powder particles by improving the geometrical parameters like standoff distance and powder shape and size range in CS coating process technology. This analysis was carried out with constant parameters which include propelling gas mixture, particle size range, pressure conditions, temperature conditions at inlet and outlet sections, etc. The best-suited shape of powder particles and standoff distance based upon the simulation results was discussed.

## 2 Model, Material, and Methodology

### *2.1 Geometry*

The geometry required for the simulation of the CS process technology should have the same arrangement as that of the experimental model. The geometry used in this simulation process had been drawn using SolidWorks software, which consists of an injector-nozzle arrangement, the substrate has been placed in front of the nozzle outlet on the same axis as the nozzle, and the arrangement is made known in Fig. 1. The nozzle used in this work is of the circular cross-sectional area with diameters of 19 mm, 3 mm, and 7 mm at inlet, throat, and outlet, respectively. The length of the convergent-divergent nozzle has been taken as 230 mm with 55 mm convergent part and 175 mm divergent part. The barrel has been placed at the inlet of the convergent part of diameter 19 mm with 15 mm length. The injector has been positioned at the inlet of the nozzle of 2.5 mm diameter and 30 mm in length. A circular plate shape substrate, with 6 mm thickness and 60 mm diameter, has been placed in front of the nozzle outlet. All the parts of the geometry have been designed to simulate the work in 2D and using symmetry to reduce the computational time.

### *2.2 Computational Field and Boundary Condition*

The computational field with boundary conditions with all the phases and domains has been demonstrated in Fig. 2. The geometry has been converted into several elements and nodes of quadrilaterals. The CFD analysis has been carried out using standoff distances of 15 mm, 25 mm, 35 mm, and 45 mm having 90,579, 92,499, 93,174, and 90,578 nodes, respectively. The geometry with 25 mm of standoff distance has been employed for the analysis of different particle shapes and size range. The CFD

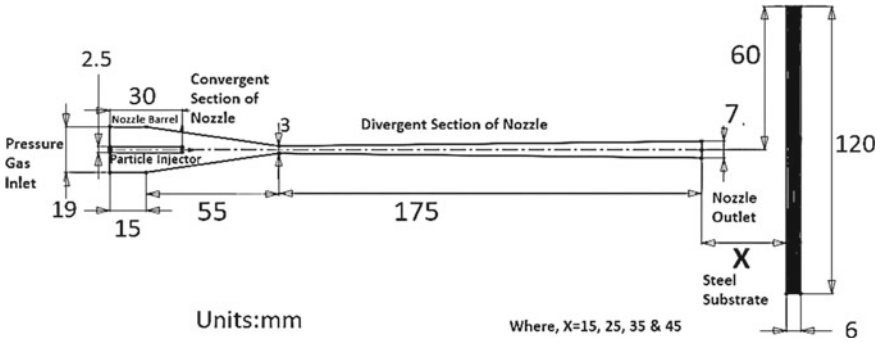


**Fig. 1** Geometry with standoff distance ($X = 15$ mm, 25 mm, 35 mm, and 45 mm)

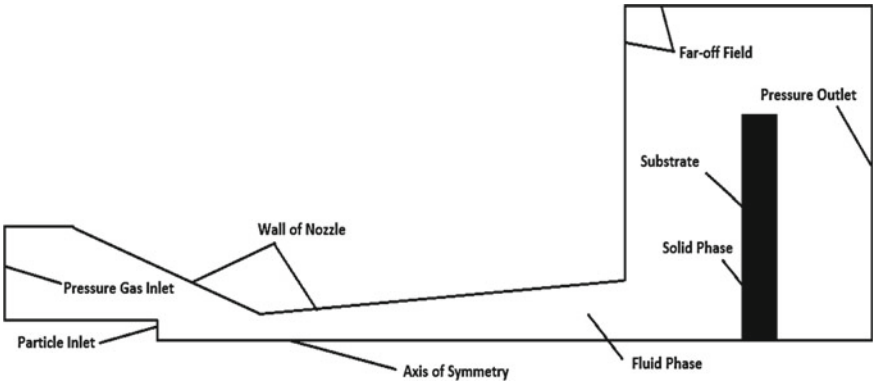


**Fig. 2** Boundary conditions for CS coating CFD simulation

simulation meshing has been shown in Fig. 3, the chief regions which include the symmetry, the outlet of the nozzle including the substrate, throat area and inlet of the nozzle had been displayed separately via Fig. 3a–d, respectively.

## *2.3 Governing Equations and Material Properties*

The gas phase is governed by ideal gas law by considering the compressibility effect. The gas flow embraces the continuity equations, energy equations, and momentum equations predominant to the flow of gases. The gases used in this simulation process have a mixture of nitrogen and helium, and the mixture of nitrogen and helium has been taken in the ratio of 4:6 ($N_2$: He). The powder particles have been kept as copper metal with different shapes and sizes, having a density of 8978 kg/m$^3$ and specific heat (Cp) of 381 J/Kg K. The shape of powder particles has been taken as spherical and non-spherical (SF = 0.8) (crushed sandstone shape) [31] with a size range of

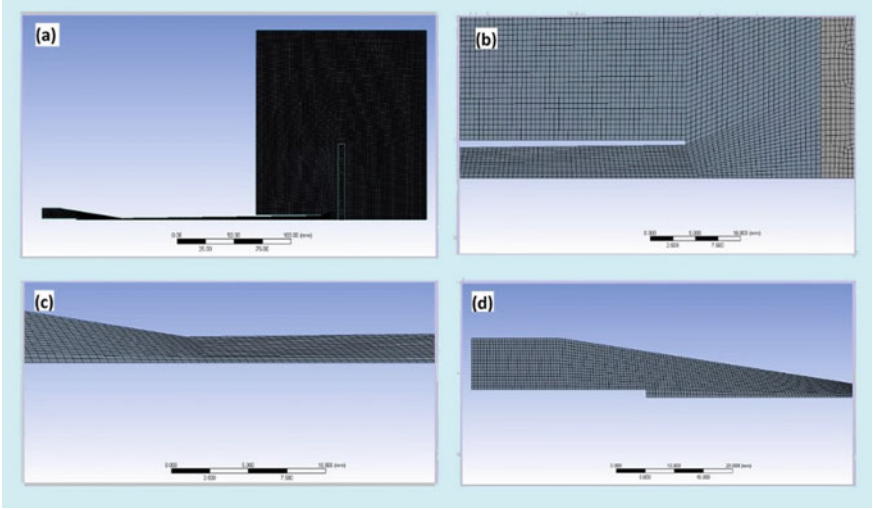


**Fig. 3** CFD simulation mesh: **a** meshing of geometry, **b** meshing at nozzle outlet/near the substrate, **c** meshing at the nozzle throat, and **d** meshing at the particle and gas inlet

15–60 μm using the rosin-rammler method with the mean particle size of 30 μm and injected with the temperature of 300 K. The substrate material has been taken as steel at the temperature of 300 K, with density, specific heat (Cp), and the thermal conductivity of 8030 kg/m$^3$, 502.48 J/kg K, and 16.27 W/m K, respectively.

## *2.4 Numerical Simulation*

The CFD analysis, employing the ANSYS software, has been carried out to escalate the role of particle shape and size and the effect of standoff distance before impact. The temperature and pressure of the propelling gas at the gas inlet are 675 K and 15 bar, whilst at particle, inlet has been taken as 325 K and 1 bar.

The simulation of CS process technology has been carried out using the pressure-based, axisymmetric model. The numerical simulation model has been taken as the two-equation realizable k-ε model with standard wall function, as this model is the most realistic as compared to other available models.

## 3 Outcomes and Discussion

Interpreting to the prior research work [14, 27], the pressure taken was 3–7 MPa to obtain the optimal impact velocity of particles having a diameter of 10 μm. Whereas, in the present study, the pressure is taken as 15 bar or 1.5 MPa with varying particle size and shape of powder particles. Consequently, this study implies the idea of shape effect on impact velocity accompanied by particle size. Secondly, the effect of particle shape on temperature and impact velocity is investigated.

### *3.1 Effect of Shape and Size on Impact Velocity and Temperature*

The impact velocity and temperature simulation analysis for two different shapes of particles and size range upon impact velocity and temperature have been shown by Figs. 4 and 5. The simulation results are plotted in Figs. 6 and 9, and the velocity and temperature of the spherical-shaped particle found higher as compare to non-spherical, which shows that spherical shape of powder particles will certainly affect the coating quality in terms of porosity, hardness, and bond strength as compare to non-spherical shape powder particles, because of the velocity and temperature difference and shape difference. The impact velocity and temp. of the particles before impact have been indicated by the data label in Figs. 6 and 7 in which the velocities of spherical and non-spherical particles just before impact upon the substrate have been

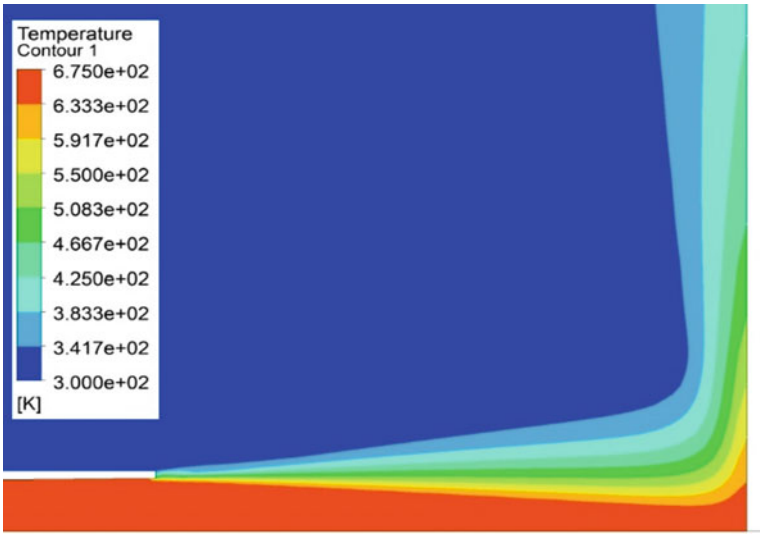


**Fig. 4** Temperature contour near the substrate


**Fig. 5** Velocity contour near the substrate

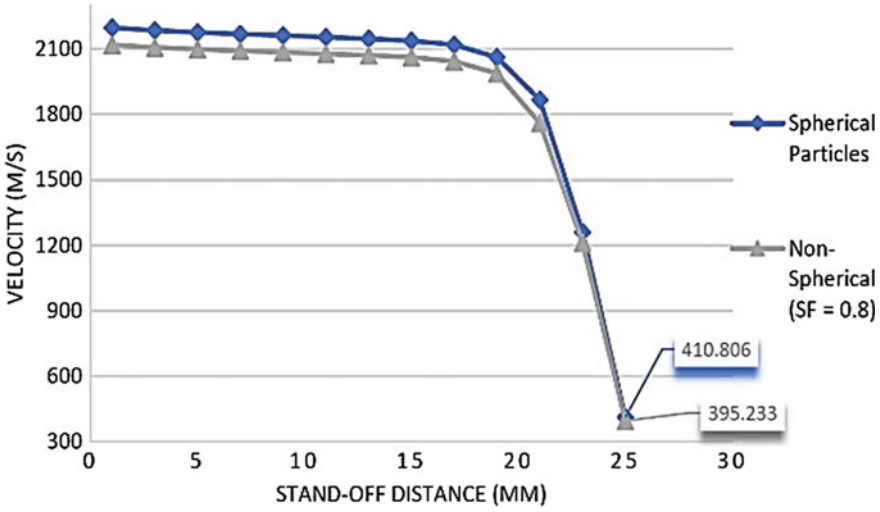


**Fig. 6** Effect of particle shape on velocity

recorded as 1259.03 and 1211.87 m/s. The final impact velocity of spherical and non-spherical particles was 410.806 and 395.233 m/s. The temperature of spherical and non-spherical particles is 671.06 K and 621.81 K at the substrate. This indicates that

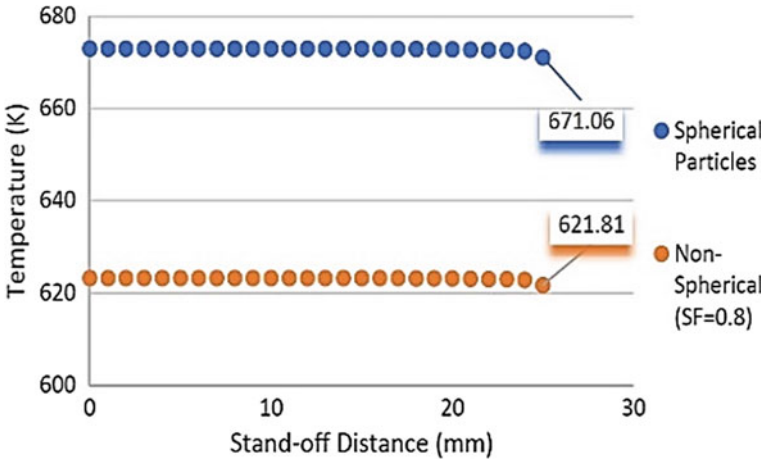


**Fig. 7** Effect of particle shape on temperature

the spherical particles strike with high velocity and temperature as compare to non-spherical ones. All the simulations of different particle shapes have been performed using geometry with a 25 mm standoff distance.

## *3.2 Effect of Standoff Distance on Impact Velocity and Temperature*

The analysis of standoff distance upon impact velocity and temperature of powder particles gives the results as shown in Figs. 8 and 9, in which the velocities 1234.84 m/s, 1259.03 m/s, 1325.06 m/s, and 1110.85 m/s were found for 15 mm, 25 mm, 35 mm, and 45 mm standoff distance, respectively. The final impact velocity of spherical and non-spherical particles was 403.806 m/s, 4010.806, 443.216, and 381.448 m/s for 15, 25, 35, and 45 mm standoff distances, respectively, upon which the particle gets impacted on the substrate surface. The temperature behaves in ascending order with that of standoff distance. The velocity before impact indicates the difference and found to be best with 35 mm standoff distance and lowest with 45 mm standoff distance. Considering velocity and temperature 35 mm standoff distance found efficient for CS coating.

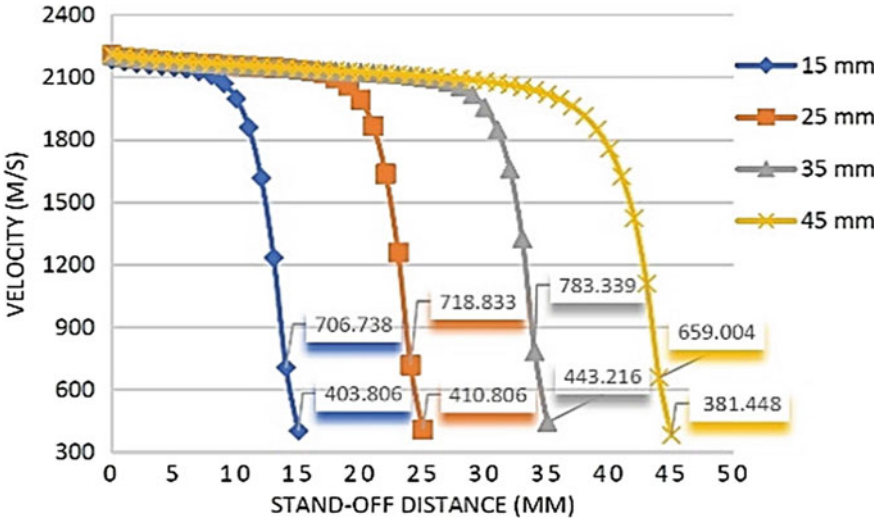


**Fig. 8** Effect of standoff distance on velocity

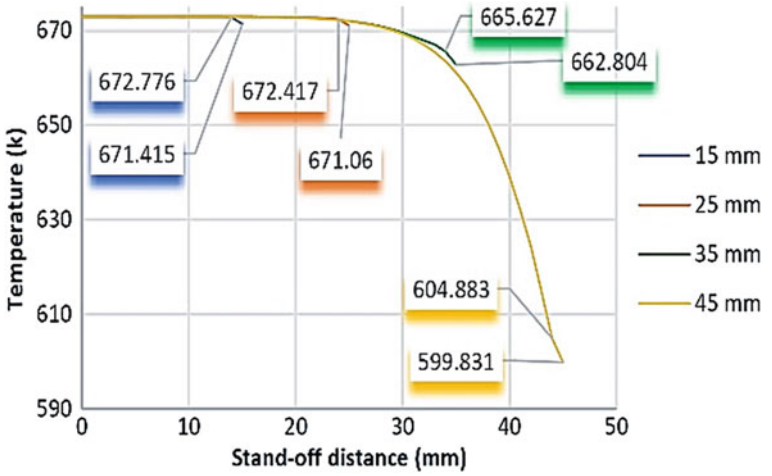


**Fig. 9** Effect of standoff distance on temperature

## 4 Conclusion

The research findings to analyze the effect of particle shape and size on impact velocity and temperature and also the role of standoff distance in CS process technology indicates that:

1. The impact velocity and temperature of spherical-shaped particles are high as compare to the non-spherical shape (SF = 0.8) of particles.
2. The spherical shape of powder particles with a standoff distance of 35 mm is optimum to use in CS coating.
3. The standoff distance higher than and lower than that of findings, affect the coating in terms of its properties, porosity, bond strength, and efficiency.

## References

1. Yin S, Cavaliere P, Aldwell B, Jenkins R, Liao H, Li W, Lupoi R (2018) Cold spray additive manufacturing and repair: fundamentals and applications. Addit Manuf 21:628–650
2. Liu Z, Wang H, Haché MJR, Chu X, Irissou E, Zou Y (2020) Prediction of heterogeneous microstructural evolution in cold sprayed copper coatings using local Zener-Hollomon parameter and strain. Acta Mater 193:191–201
3. Yeom H, Sridharan K (2021) Cold spray technology in nuclear energy applications: a review of recent advances. Ann Nucl Energy 150:107835
4. Pattison J, Celotto S, Morgan R, Bray M, O'Neill W (2007) Cold gas dynamic manufacturing: A non-thermal approach to freeform fabrication. Int J Mach Tools Manuf 47:627–634
5. Kumar M, Singh H, Singh N (2020) Effect of increase in nano-particle addition on mechanical and microstructural behaviour of HVOF and cold-spray Ni-20Cr coatings on boiler steels. Mater Today Proc 21:2035–2042
6. Das P, Bandyopadhyay PP, Paul S (2019) Finish form grinding of thermally sprayed nanostructured coatings. Adv Mater Process Technol 5:39–52
7. Klinkov SV, Kosarev VF, Shikalov VS, Vidyuk TM, Chesnokov AE, Smirnov AV (2019) Influence of preliminary heat treatment and ball milling of copper powder on cold spray process. Mater Today Proc 25:360–362
8. Winnicki M, Kozerski S, Małachowska A, Pawłowski L, Rutkowska-Gorczyca M (2021) Optimization of ceramic content in nickel–alumina composite coatings obtained by low pressure cold spraying. Surf Coatings Technol 405
9. Vilardell AM, Cinca N, Cano IG, Concustell A, Dosta S, Guilemany JM, Estradé S, Peiró F (2016) Dense nanostructured calcium phosphate coating on titanium by cold spray. J Eur Ceram Soc
10. Cao K, Yu M, Liang CM, Chen H (2020) Quantitative determination of SiC particles distribution of cold sprayed Al5056/SiC composite coatings. Surf Eng 36:1040–1048
11. Zhao P, Zhang Q, Guo Y, Liu H, Deng Z (2020) Atomic simulation of crystal orientation effect on coating surface generation mechanisms in cold spray. Comput Mater Sci 184:109859
12. Jami H, Jabbarzadeh A (2020) Molecular simulation of high-velocity deposition of Titanium dioxide nanoparticles on titanium. Appl Surf Sci 542:148567
13. Oyinbo ST, Jen TC, Zhu Y, Ajiboye JS, Ismail SO (2020) Atomistic simulations of interfacial deformation and bonding mechanism of Pd-Cu composite metal membrane using cold gas dynamic spray process. Vacuum 182:109779
14. Khan M, Zunaid M, Murtaza Q (2020) Examination of titanium powder with different particle sizes for velocity. Mater Today Proc 29:1–5
15. Wu H, Huang C, Xie X, Liu S, Wu T, Niendorf T, Xie Y, Deng C, Liu M, Liao H, Deng S (2020) Influence of spray trajectories on characteristics of cold-sprayed copper deposits. Surf Coat Technol 405:126703
16. Chakrabarty R, Song J (2020) A modified Johnson-Cook material model with strain gradient plasticity consideration for numerical simulation of cold spray process. Surf Coat Technol 397:125981

17. Kumar S, Zunaid M, Murtaza Q, Ansari N, Arora A (2015) Simulation of Injector in Cold Spray Process by Fluent-6. In: International conference on advanced research in innovation, pp 464–472
18. Singh S, Singh P, Singh H, Buddu RK (2019) Characterization and comparison of copper coatings developed by low pressure cold spraying and laser cladding techniques. Mater Today Proc 18:830–840
19. Kumar AS, Kar S, Bandyopadhyay PP, Paul S (2018) Grinding of ceramics-sintered ceramics versus ceramic coatings. Adv Mater Process Technol 4:538–547
20. Reddy BVR, Kummitha OR (2017) Characterization of spray formed and cold rolled Al–Pb alloy. Mater Today Proc 4:267–276
21. Das B, Bandyopadhyay PP, Nath AK (2018) An investigation on corrosion resistance and mechanical properties of laser remelted flame sprayed coating. Adv Mater Process Technol 4:660–668
22. Chakrabarty R, Song J (2020) Numerical simulations of ceramic deposition and retention in metal-ceramic composite cold spray. Surf Coat Technol 385:125324
23. Seraj RA, Abdollah-Zadeh A, Assadi H, Hajipour H, Kadkhodaee M (2020) Effect of substrate on the properties of cold sprayed coating of WC-10Ni. Adv Mater Process Technol 00:1–14
24. Tripathy S, Behera A, Pati S, Roy S (2020) Corrosion resistant nickel coating on mild steel by cold gas dynamic spraying. Mater Today Proc
25. Sabanayagam S, Chockalingam S (2020) Analysis of high temperature oxidation behaviour of SS316 by Al2O3 and Cr2O3 coating. Mater Today Proc 3–7
26. Mindivan F, Mindivan H (2016) Surface properties and tribocorrosion behaviour of a thermal sprayed martensitic stainless steel coating after pulsed plasma nitriding process. Adv Mater Process Technol 2:514–526
27. Khan M, Zunaid M, Murtaza Q (2021) Simulation of cold spray coating for powder pre-heat and impact velocity. Mater Today Proc. https://doi.org/10.1016/j.matpr.2021.01.780
28. Hemeda AA, Zhang C, Hu XY, Fukuda D, Cote D, Nault IM, Nardi A, Champagne VK, Ma Y, Palko JW (2020) Particle-based simulation of cold spray: influence of oxide layer on impact process. AdditManuf 101517
29. Kumar A, Nayak SK, Bijalwan P, Dutta M, Banerjee A, Laha T (2019) Mechanical and corrosion properties of plasma-sprayed Fe-based amorphous/nanocrystalline composite coating. Adv Mater Process Technol 5:371–377
30. Rutkowska-Gorczyca M (2020) X-ray diffraction and microstructural analysis of Cu–TiO2 layers deposited by cold spray. Mater Sci Technol (United Kingdom) 0836
31. Wang D, Fan LS (2013) Particle characterization and behavior relevant to fluidized bed combustion and gasification systems. In: Fluidized bed technologies for near-zero emission combustion and gasification, pp 42–76